THE 9TH JULY 1998 FAIAL EARTHQUAKE: COMPARISON OF STOCHASTIC FINITE FAULT DAMAGE SIMULATION WITH SURVEYED DATA

G. Zonno, G. Musacchio & F. Meroni

Istituto Nazionale di Geofísica e Vulcanologia, Sezione di Milano-Pavia, Italy

C. S. Oliveira, M. A. Ferreira & F. Neves

Instituto Superior Técnico, Departamento de Engenharia Civil e Arquitectura, Lisbon, Portugal

SUMMARY

The Azores earthquake, July 9, 1998 (M_w 6.2) caused a large damage to the stock of old masonry buildings, with maximum felt intensity I_s=VIII (MMI). A stochastic strong ground motion (SM) was simulated on the islands struck by the earthquake using published fault solution, to derive maps of average Peak Ground Acceleration (PGA) at bedrock. Detailed analysis was done at the Horta station comparing stochastic-computed and observed PGA, PGV, Response Acceleration Spectra and Response Spectrum Intensity (SI) values.

Although recordings on Faial (Horta) and Terceira Islands are not enough to fully constrain the simulation parameters, they can define the range of possible variation. Relationships between PGA and MMI were used to retrieve intensity. Retrieved and observed intensities allowed to derive an average damage index according to the EMS-98 classification.

1. INTRODUCTION

The Azores archipelago is the morphologic expression at surface of the interaction between the triple junction of three large tectonic plates, the North American, Eurasian and African plates, and a hot-spot located in a slow-moving plate (e.g.: Silveira *et al*., 2006; Yang *et al*., 2006; Schilling, 1991).

As a result of its location on active plate boundaries, the archipelago is subject to frequent seismic activity revealed by low-magnitude seismic sequences that occasionally are triggered by moderate to large earthquakes. In the dawn of July 1998 a M_w=6.2 earthquake struck the island of Faial causing, in the northeastern part of the island, major destruction affecting more than 5000 people, 8 deaths, 150 persons injured and 1500 homeless (Senos *et al*., 1998). The main shock was located offshore, 8 km NE of the Island (Matias *et al*., 2007) and triggered a seismic sequence that lasted for several weeks.

The observed intensity is influenced both by site effects related to thick layers of soft sediments and pyroclastic deposits, and by high vulnerability of constructions. The maximum felt intensity (Modified Mercalli Scale) was VIII, in Northeastern part of Faial Island (Matias *et al*., 2007) possibly related to amplification of shaking caused by soft rocks (Senos *et al*., 1998; Madeira, 1998). Damage to monumental structures and road network was observed mostly near the epicentre. The high destruction observed in Faial and Pico revealed a total of 2100 buildings with partial or total collapse located up to 30 km from the epicentre, which is related to the high vulnerability of the predominant type of construction.

Ten years later the huge amount of information and collected data allow a better understanding of pending questions on the Faial 1998 earthquake and the related damage. A stochastic ground motion simulation was developed, using as input data the fault parameters and the moment magnitude to derive damage scenarios from peak ground acceleration (PGA). Although classical vulnerability and damage models are based on the macroseismic intensity, recent models require seismic input derived from instrumental data.

In this work we compare damage models derived from the two different approaches. We use macroseismic data collected in the field survey carried out after the 1998 earthquake, and compute seismic scenarios; damage scenarios as a function of intensity are compared with observed damage.

1.1. Geologic setting

The Azores plateau is a region of a triangular shaped anomalously shallow bathymetry within the Atlantic Ocean (Figure 1), on top of which has emerged a volcanic archipelago, still active today. The complex morphology of the plateau clearly reflects the interaction of intense magmatic and seismic activity. Indeed, the central and eastern islands marks the boundary between the Eurasian and Africa plates, along the Azores-Gibraltar Fault Zone (Madeira, 1998; Lourenço *et al*., 1998), an oblique spreading centre and broad sheared region under transtensile stress regime and an abnormally thick oceanic crust.

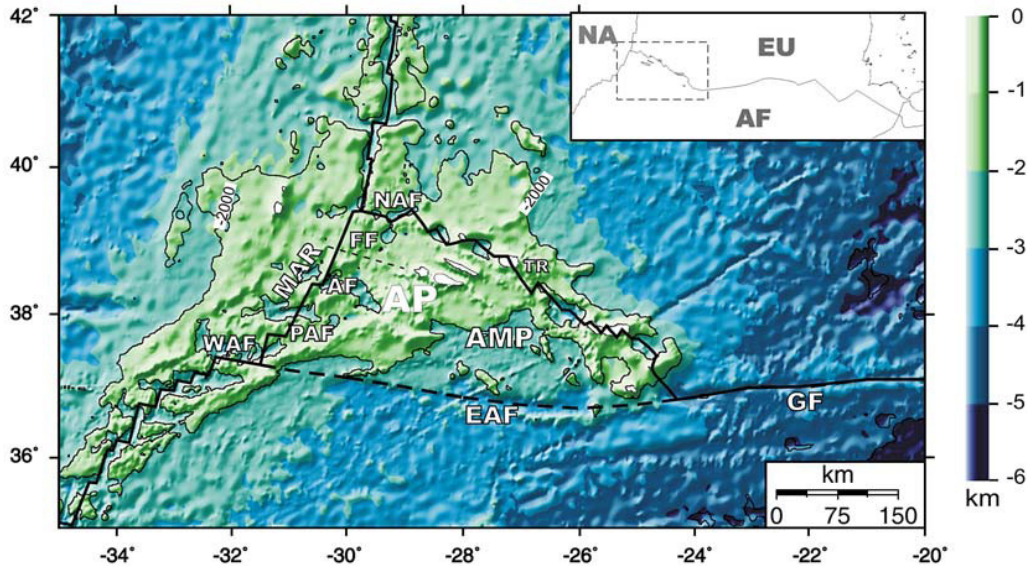

Figure 1: The main tectonic features for the Azores region. MAR=Mid-Atlantic Ridge; TR=Terceira Ridge; NAF=North Azores Fracture Zone; FF=Faial fracture; AF=Azores fracture; PAF=Princess Alice fracture; WAF=West Azores fracture; EAF=East Azores fracture; GF=Gloria Fault; AP=Azores plateau; NA=North American plate; EA=Eurasian plate; AF=African plate. The bathymetric lines are taken from the digital bathymetric data set ETOPO2 (U.S. Department of Commerce, NOAA/NGDC, 2001). The marked black line is the 2000m isoline that bounds the plateau. (from Borges *et al*., 2007, and references therein)

1.1.1. Tectonic setting and seismicity

In the Central Azores Islands (Faial, Pico and S Jorge) the plateau seafloor is a 1200m bsl flat region, elevated relative to the adjacent eastern and western islands (Lourenço *et al*. 1998), where the islands are the emerging portion of WNW-ESE trending ridges (Vogt, 1976; Dias *et al*., 2007) parallel to the plates boundary.

Three fault systems (Figure 2) cluster most of the seismicity and volcanisms in the islands. A WNW–ESE (N60-80W) dextral strike-slip system plunges 60° or 80° to NNE or SSW, controls the shape of the islands and of the main ridges. A NNW–SSE (N10-30W) conjugated left strike-slip system plunging 60° to 90° to WSW or to ENE is less prominent (Madeira *et al*., 2003). NE–SW trending faults are also present, but their meaning is not yet understood.

Observation of striated fault surfaces indicates that, besides oblique slip, strain partitioning may occur at the fault zone scale and strike to normal components may be separated in time or space. The occurrence in the archipelago of earthquakes with normal and strike slip focal mechanisms in parallel faults, separated by a few or tens of kilometres, suggests that strain partitioning may also occur at the regional scale (Madeira, 1998).

The faults geometry and kinematics indicate a stress field with the minimum horizontal compressive stress axis ($\sigma 3$) trending NE-SW. However, permutations between maximum ($\sigma 1$) and intermediate ($\sigma 2$) compressive stress axis (NW-SE horizontal, and vertical, respectively), may originate transtensile or tensile regimes (Reches, 1983) and trigger alternating phases of intense tectonic activity and volcanism.

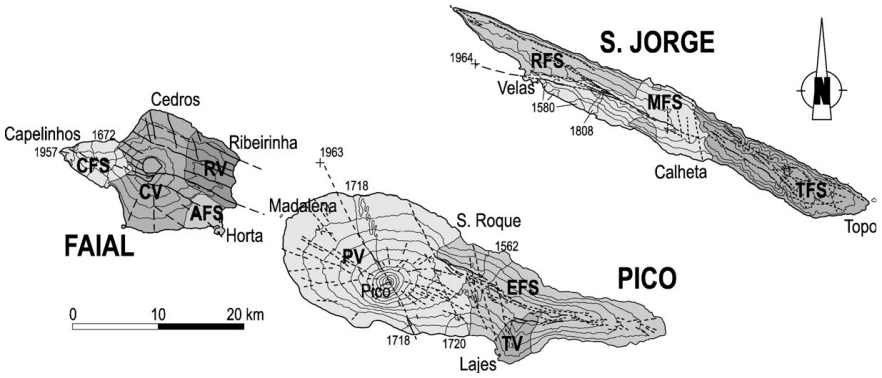

Figure 2: Simplified geology of the islands of Faial, Pico and S. Jorge. Different shades of grey indicate the location of the main volcanic units; black lines are faults; arrows point to the main dextral and conjugate left strike-slip fault systems. Volcanic units in Faial: RV — Ribeirinha volcano; CV — Caldeira Volcano; AFS — Almoxarife fissural system; CFS — Capelo fissural system. Volcanic units in Pico: TV—Topo volcano; EFS—Eastern fissural system; PV—Pico Volcano. Volcanic units in S. Jorge: TFS— Topo fissural system; RFS — Rosais fissural system; MFS — Manadas fissural system. Historic eruptions are indicated by dates. (Dias *et al*., 2007, redrawn)

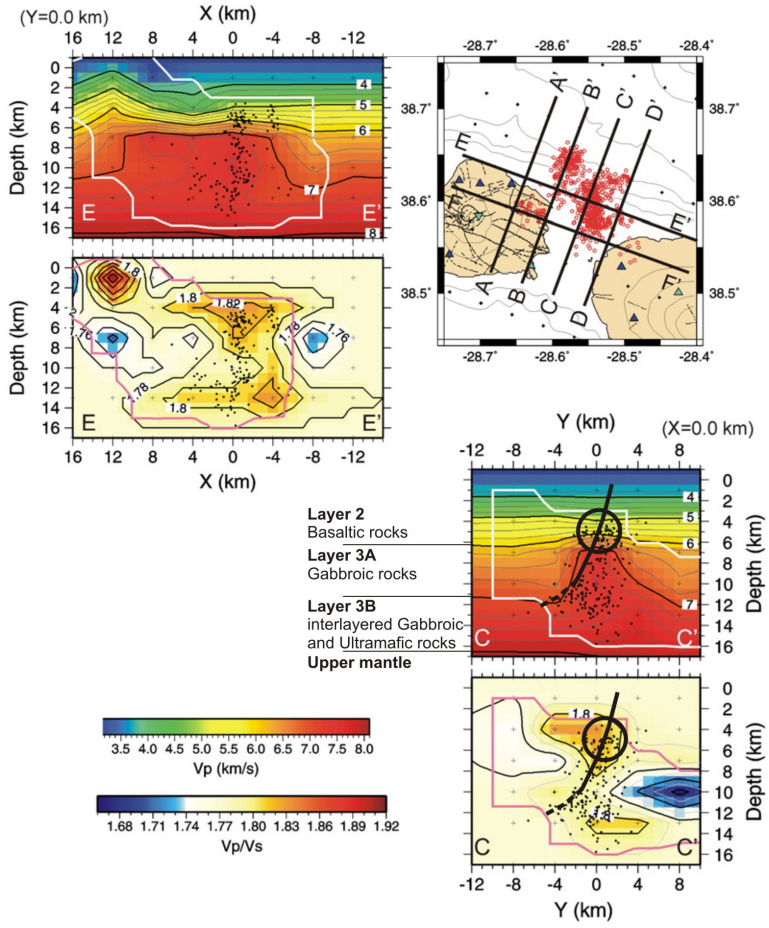

Figure 3: Vertical cross sections of the Vp and Vp/Vs models (Dias *et al*., 2007, redrawn). Only two of the profiles marked in the central map and published in Dias *et al*. (2007) are shown. Each cross section represents the Vp model on top of the Vp/Vs. Hypocenters (dots) are represented in slices 1 km thick. Good and intermediate resolved areas were delimited by white (Vp) and pink (Vp/Vs) lines. Petrological interpretation is from Matias *et al*., (2007). Thick black line and circle highlight the fault that ruptured during the July 1998 earthquake

1.1.2. The 1998 Faial earthquake

The 1998 Faial earthquake had its epicentre 8 km NE of Faial Island (Borges *et al*., 2007), where seismicity occurs on strike-slip NW–SE trending lineaments, according to a NE-SW trending σ3. The plane that ruptured in 1998 had azimuth=156°, dip=85°, and left-lateral strike–slip motion. A very wide dispersion of locations was issued by the worldwide networks and persisted even after a compilation of large sets of phase readings. This is due to the unfitness of the velocity model and/or location procedure for this particular region of the Earth. The focal depth published in the literature based on different approaches is relatively shallow, less than 10 km, in agreement with the oceanic-type crust. Main shock relocation based on a 1D velocity model suggests epicentre at Latitude 38.634°N, Longitude 28.523°W (EPI 1), and hypocenter between 2 and 5 km. Epicentre EPI 2 (Latitude 38.640°N, Longitude 28.590°W) was issued by SIVISA a few hours after the earthquake, based on the Azores local network, and was revised by Oliveira (adapted from Madeira, 1998). Moreover detailed seismic tomography (Dias *et al*., 2007) allows to infer that the July 1998 main shock occurred at a depth between 4 and 6 km, flanking the northeast boundary of a large gabbroic intrusion. High V_P gradients reveal the presence of the fault, while high V_P/V_S, translates into reological changes associated with slip movement on the fault (Figure 3). Density was inferred to be about 2.8 g/cm^3 based on physical properties rocks (Carmichael, 1990) supposed to occur at hypocentral depth.

2. AVAILABLE DATA

The July 9 1998 event caused relatively large ground-shaking (PGA= 0.39 g) at the Prince of Monaco Observatory on the top of a scoria cone in Horta town (Faial island). However relatively low damage was at odd with this large PGA value. Stock of houses in the nearby city of Horta (about 3 km from the Observatório) were not heavily damaged whereas high destruction of buildings was observed at relatively large distance from the epicentre (Matias *et al*., 2007). Pronounced site-effects might have caused large amplifications on ground shaking. However, recent modelling of existing simple structures response in the city of Horta (Oliveira *et al*., 2001) infers PGA values (0.2 to 0.25 g) more consistent with the observed damage in the city. Ground motion recordings at Terceira (GZC, SEB and PVI stations, at 113-133 km) and S. Miguel islands (MOS station at 250 km), show much lower shaking (3-16 mg).

Recordings at Horta station were used to constraint model parameters such as response acceleration spectra and the high frequency spectral decay parameter, *k* (Anderson *et al*., 1984). Low PGA values at Terceira and S. Miguel islands were used as qualitative constraints for the far field simulations.

Table 1 - 9th July 1988 Faial Earthquake locations coordinates, recorded PGA ranges at each site, and epicentre-stations distance for EPI 1 (Matias *et al*. 2007) and EPI 2 (Oliveira, adapted from Madeira *et al.*, 1998)

				Epicentre EPI 1 Lat. 38.634; Long. -28.523	Epicentre EPI 2 Lat. 38.640; Long. -28.590
Code station	Lat.	Long	PGA (mg)	Distance (km)	Distance (km)
HORTA (Faial)	38.529	-28.63	~ 327 - 400	14.88	12.77
GZC (Terceira)	38.657	-27.22	~ 12 – 14	113.25	119.05
SEB (Terceira)	38.668	-27.09	~ 9 – 23	124.68	130.47
PVI (Terceira)	38.732	-27.06	~ 5 – 10	127.52	133.25
MOS (S. Miguel)	37.890	-25.82	~ 3 – 5	248.99	254.68

The maximum intensity Modified Mercalli Scale (MMI) caused by the 1998 Faial earthquake was VIII, observed in the Northeastern portion of Faial island. The earthquake was felt in Pico and S. Jorge islands, where maximum intensities reached VII and V, respectively (Figure 4).

Inhomogeneous distribution of vulnerability reveals that areas were 90% of buildings collapsed are juxtaposed next to areas where likely well-built masonry buildings only suffered cracks opening. Therefore macroseismic observations were strongly influenced by site-effects related to the occurrence of hard lava-flows rocks adjacent to soft ignimbrite deposits (Figure 4). Likely, intensities ranging from VII to VIII observed in the north east portion of Faial Island are attributed to local amplification effects caused by soft sediments and/or topographic effects on the wave field. In the northwest portion of Pico, at similar distance from the epicentre, intensities ranging from V to VI could be more representative of shaking at bedrock.

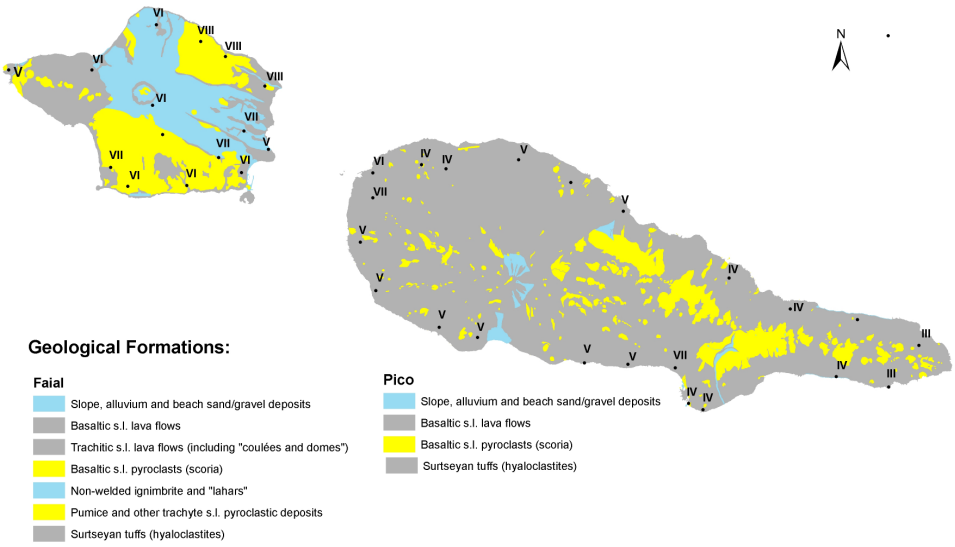

Figure 4: Lithological map of the Faial and Pico islands and observed intensities (Modified Mercalli Intensity scale) from Matias *et al*. (2007)

3. FINITE FAULT GROUND MOTION SIMULATION

We study ground motion using a finite-fault stochastic simulation method computed with the code EXSIM (Motazedian and Atkinson, 2005). This code, being an extension of the stochastic point source simulation method of Boore (2003), offers several significant advantages over previous stochastic finite-fault release (i.e. FINSIM; Beresnev and Atkinson, 1998; Berardi *et al*., 2000; Carvalho *et al*., 2008; Castro *et al*., 2008). The fault plane is assumed to be a rectangle broken into an appropriate number of sub-faults, which are modelled as point sources. The sub-faults have ω^2 spectra, their size defines the moment and corner frequency, while the number of triggered sub-faults is adjusted to reach a specified target moment.

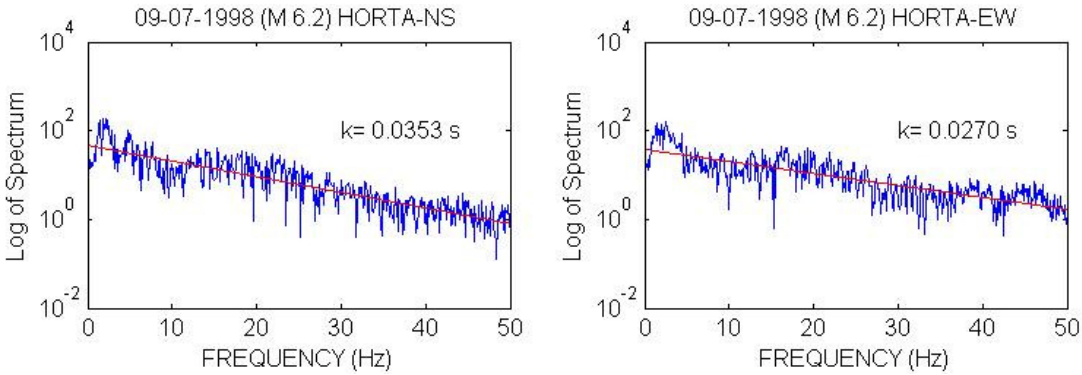

Figure 5: Frequency Power Spectra for horizontal components (NS and EW) accelerograms at Horta site. The k value used for the simulation is assumed to be the mean value of 0.03.

The approach, merely kinematics, does not describe the physics of the rupture but is a preliminary estimate of ground shaking in terms of PGA. We did not have enough number of recordings to allow highly constrained ground-shaking analysis, since only one accelerogram of the 1998 Faial earthquake exists. Therefore some of the parameters used in the stochastic modelling had to be defined making simple assumptions and using available published information.

3.1. Modelling parameters

The finite-fault model parameters require specification of (1) the fault-plane geometry (length, the width and orientation), (2) the source (slip distribution, stress drop, nucleation point, rupture velocity) and (3) the crustal properties of the region (geometric spreading coefficient, quality factor Q(f), etc.). We compute ground motion at bedrock for two possible epicentre locations, EPI 1 and EPI 2 (Table 1), neglecting site-specific soil response. The fault-plane geometry includes a length of 16.5 km and a width of 9.4 km, derived from the Wells and Coppersmith (1994) relationship for a M 6.2 event; and an attitude with 165° strike and 85° dip. The number of sub-faults (9 along length and 5 along width) were set to have almost squared dimensions, while the depth to the upper edge equal to 1.1 km was derived from published seismological studies (Matias *et al*., 2007; Dias *et al*. 2007). The source characteristics were defined assuming two different slip models (automatic random and Gaussian distribution) computed on given nucleation points for a 6.2 moment magnitude, a stress drop equal to 200 bars and a rupture velocity on the fault equal to 0.8 of the shear wave velocity. We assumed a stress drop equal to 200 bars, which is consistent with that derived from P-waves spectral analysis (Borges *et al*., 2007) and with a 200 bars deviatory stress at 5 km depth (Matias *et al*., 2007).

Table 2 - Faial earthquake simulation parameters

Parameter	Parameter value		Parameter	Parameter value
Moment Magnitude	6.2		k	0.03 sec
Fault orientation	Strike 165°, dip 85°		Q(f)	$239.0*f^{1.06}$
Depth of top	1.1 km		Stress drop	200 bar
Fault dimensions	Length (width) 16.5 (9.4) km		Geometrical attenuation	If R < 30, R^{-1}; else $R^{-0.5}$
Number of sub faults	Along length 9, along width 5		distance-dependent duration	To + 0.1 R (sec)
FFT points,	16384		Windowing function	Saragoni-Hart
Sample interval	0.005 sec		Amplification function	No applied
Shear wave velocity	3.5 km/sec,		Slip model	Random and Gaussian
Density	2.8 g/cm^3		DynamicFlag and Pulsing (%)	1 and 50.0
Rupture velocity	0.8 x shear wave velocity		Damping	5% of critical damping

Although geometrical spreading coefficient and the quality factor Q(f) are crucial to ground-shaking simulation we do not have attenuation information specific to the studied area. Nevertheless we tried to constrain Q using values proposed for areas having similar geodynamic setting. Therefore we use Q equal to 239 within the average proposed for South Iceland (Olafsson *et al*., 1998) where values ranges between 128 and 425. We assumed a relationship $Q(f)=Qo*f^{\theta}$ with Qo = 239 and a θ = 1.06. This assumption causes an almost linear frequency-dependent quality factor Q(f) that in turns results into a PGA at Terceira within the range of recorded values. The same relationship Q(f), used in this study, was used for earthquake shaking scenarios in the Lisbon area (Carvalho *et al*., 2008).

The distance-dependent duration (To + 0.1R, with To=4.0) was selected according to other previous simulation study and validated with the average duration of horizontal components at the Horta station. A summary of all parameters used to generate PGA and intensity maps are listed in Table 2.

To investigate the uncertainty on the assumptions we performed a parametric study at the Horta site that will be discussed later on.

3.2. Relationships between shaking parameters and intensity

We use the relationships between MMI and PGA and Peak Ground Velocity (PGV) developed by Wald *et al*., (1999).

$$I_{MM} = 3.66 \, \mathrm{Log}_{10} \, PGA - 1.66 \qquad \text{if} \quad V \leq I_{MM} \leq VIII \quad (\sigma = 1.08) \tag{1}$$

$$I_{MM} = 3.47 \, \mathrm{Log}_{10} \, PGV + 2.35 \qquad \text{if} \quad V \leq I_{MM} \leq IX \quad (\sigma = 0.98) \tag{2}$$

We infer PGA and PGV values both from response acceleration spectra PSA (5% damping) considering almost 20 trials on the stochastic computation. PGV was derived with the approximate relationship suggested by Bommer *et al*., (2006):

$$\text{PGV (cm/s)} = \text{PSA}_{(0.5\ \text{sec})} / 20\ (\text{cm/sec}^2) \tag{3}$$

We also compute the Response Spectrum Intensity (SI, Housner, 1959) defined in (Kramer, 1996) as:

$$SI(\zeta) = \int_{0.1}^{2.5} PSV(\zeta, T)dT \tag{4}$$

The Pseudo Velocity response Spectrum was considered ranging between 0.1 and 2.5 sec. The response spectrum intensity is calculated with a damping ratio of 5%. We also tested the use a relationship between the Mercalli Cancani Sieberg Intensity (I_{MCS}) and the SI (Housner) intensity, recently developed by Gallipoli *et al*., (2007) and we finally decided to avoid converting the intensity from I_{MCS} into I_{MM}.

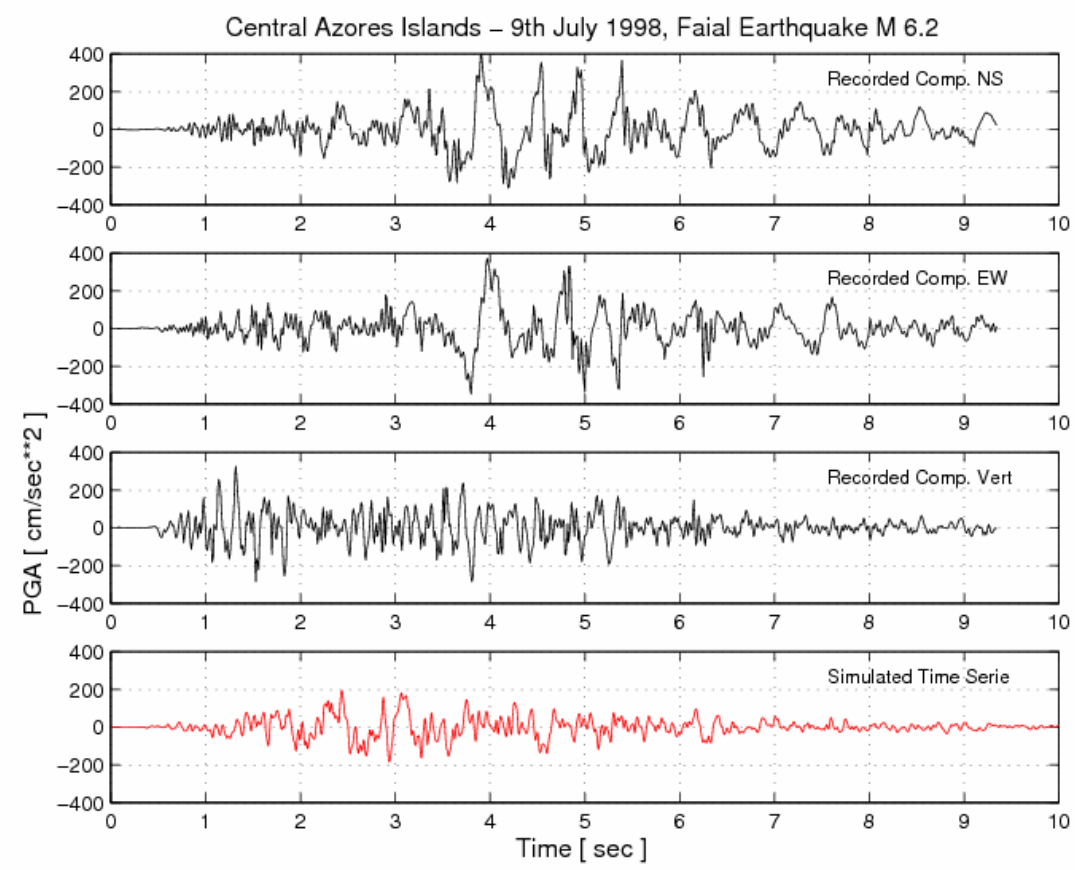

Figure 6: Top panels (black lines) are accelerometer time histories recorded at the Horta site (Faial Island). Bottom panel (red line) is the simulated accelerogram with EXSIM program. Simulation was done with EPI 2 (see Table 1), the model parameters in Table 2 and the automatic random distribution (Figure 14) with nucleation point 2 (bilateral rupture). In the distance-dependent duration model T_o = 4 sec is used.

4. EVALUATION OF FAIAL M6.2 SCENARIOS

In this study we consider two scenarios of the 9th July 1998 Faial earthquake. We use epicentre EPI 1 (Latitude 38.634°N, Longitude 28.523°W) as defined by Matias *et al*., (2007); EPI 2 (Latitude 38.640°N, Longitude

28.590°W), about 2 km closer to the Horta site, and was derived by Oliveira from damage analysis and adapted from Madeira, 1998.

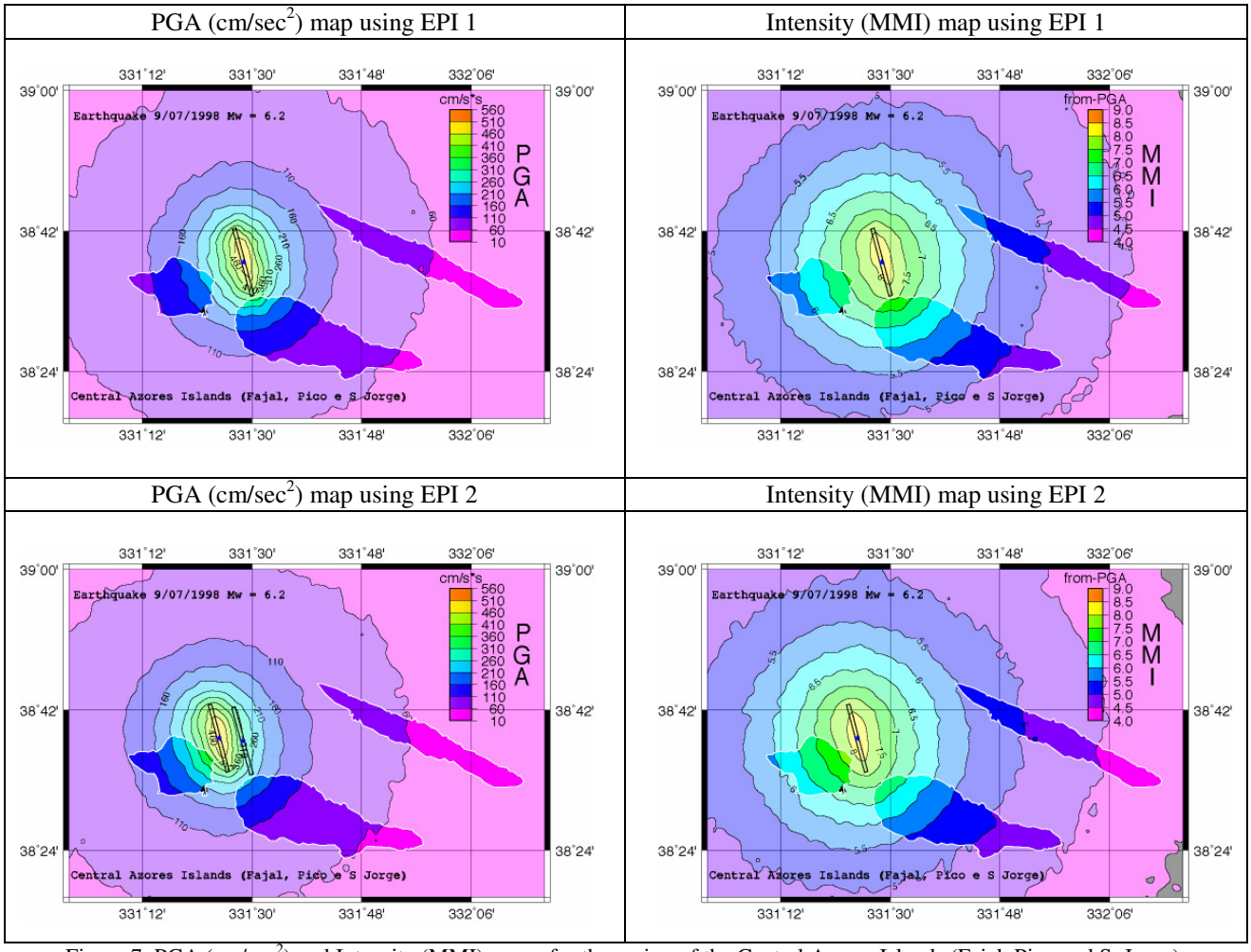

Figure 7: PGA (cm/sec^2) and Intensity (MMI) maps, for the region of the Central Azores Islands (Faial, Pico and S. Jorge). Maps were computed on a 0.02°x 0.02 grid using EXSIM and the parameters listed in Table 2. Top panels are maps computed for EPI 1; bottom panels are those with epicenter EPI 2. Relationship (1) (Wald *et al.*, 1999) was used to convert the PGA into intensity. Left bottom panel plots locations of both epicenters used for computations. Black triangle is the Horta site in the Faial island.

Depending on the epicentre location, ground shaking scenarios in terms of PGA (cm/sec^2) and intensity (MMI) result shifted by 2 km west. A visual qualitative comparison between the observed intensities (Figure 10) with the general pattern of computed intensity maps shows that EPI 2 ground shaking scenario has a better agreement with survey data.

0.75	1.13	1.20	1.21	1.20	1.17	1.07	1.00	0.75
1.01	1.52	1.61	1.62	1.61	1.58	1.44	1.35	1.01
1.12	1.74	1.79	1.78	1.74	1.68	1.59	1.49	1.12
1.01	1.52	1.61	1.62	1.61	1.58	1.44	1.35	1.01
0.75	1.13	1.20	1.21	1.20	1.17	1.07	1.00	0.75

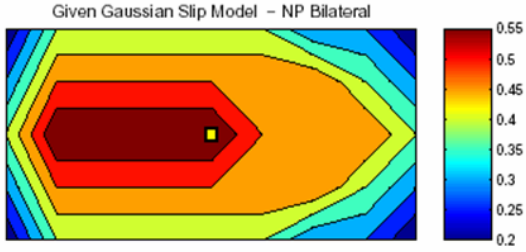

Figure 8: The slip model used to generate the PGA and Intensity maps. Left panel is the slip model input with the 45 slip weights (meter); the middle point is the selected nucleation point (gray shaded). Right panel is the output slip distributions computed by EXSIM so that total moment (M_w 6.2) is conserved.

To give a quantitative measure of the shaking differences (epicentre EPI 1 and EPI 2) we compute the stochastic intensities for each building of Faial and Pico islands and compare damage simulation with surveyed data.
In the last paragraph we will present a detailed analysis done at the Horta site comparing observed and simulated shaking parameters (PGA, PGV, Response Acceleration Spectra and Response Spectrum Intensity, SI) changing the slip distributions, the nucleation points and the quality factor Q(f).

5. COMPARISON OF RETRIEVED AND OBSERVED INTENSITIES

Table 3 summarizes the most common buildings structural system in the area of Faial and Pico.

Table 3 - Short description of common structural system in Faial and Pico islands

Construction class	Short description
CT	"construção tradicional" - known as traditional construction: the structure is mainly stone masonry with wooden floors and wooden roof
CTA	"construção tradicional alterada" - very similar to the traditional construction (structure in stone masonry and wooden roof), but part of the floors (often bathroom and kitchen) are concrete made
CM1	"construção mista 1" - structure in masonry stone, concrete floors and wooden roof
CM2	"construção mista 2" - the structure is masonry stone but there are concrete columns and beams, wooden floors, wooden roof and concrete enlargements
CM3	"construção mista 3" - concrete columns, beams and floors, either wooden or concrete roof
CC	"construção corrente" - earthquake-resistant structures, almost all elements of the house are concrete, except for the roof that might be wood

The most widely used type of construction in these islands was CT and CTA (Figure 9), highly vulnerable structures severely damaged during the earthquake.

A total of 2151 buildings in Faial and 570 in Pico had been georeferenced using GIS software. This allowed geospatial analyses to understand, for instance, the distribution of buildings damage grade with a given area. Near-faults and landslides building-by-building locations plotted on maps allow better understanding of the event dynamics.

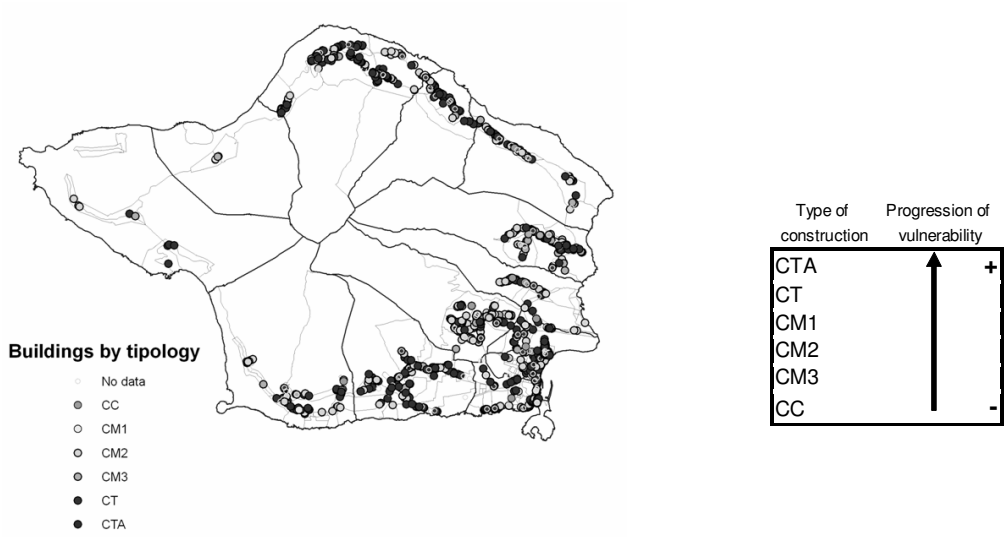

Figure 9: Left panel displays spatial buildings distribution by construction class; right panel is the relationship between construction classes and vulnerability

Figure 10 displays the macroseismic intensity distribution of the Faial earthquake expressed through Modified Mercalli Intensity scale. Left panel is based on MMI scale published by Matias *et al*., (2007); right panel is

computed by simulation of the earthquake rupture (described in Section 3 and 4). Isoseismal map has been drawn using the ArcGIS interpolation Inverse Distance Weight method (IDW) (Watson *et al*., 1985).

Figure 10: Left to right panels: MMI maps derived from (1) surveyed data (from Matias *et al*., 2007), computed using the conversion PGA -MMI (Wald *et al*., 1999), (2) for EPI1 and (3) for EPI2. The isoseismal maps were drawn using the ArcGIS interpolation Inverse Distance Weight method (IDW)

Maximum intensity observed in Faial is VIII according to MMI scale (Figure 10, left). However given the high level of destruction observed in some localities, we suggest that intensities at individual sites could have up one grade of intensity higher than regional values plotted on the map. Additional studies of microzonation (areas characterized by a homogenous seismic response) are undergoing to derive intensities using EMS-98 scale (Ferreira, 2008) directly from the observed data.

6. BUILDINGS DAMAGE ASSESSMENT

In a previous work by Ferreira (2008) evaluation of building damage was carried out according to the European Macroseismic Scale – EMS 98 (Grunthal, G., 1998). To this present study a damage scenario was estimated using the macroseismic method for vulnerability assessment (Giovinazzi and Lagomarsino, 2003) and the results can be compared with real data.

Once fixed a value to building vulnerability (V_I) and intensity I, a mean damage grade (μ_D) could be determined using the analytical function:

$$\mu_D = 2{,}5 + 3\tanh\left(\frac{I + 6{,}25V_I - 12{,}7}{3}\right) \times f(V_I, I) \tag{5}$$

Where f(V_I, I) is defined as:

$$f(V_I, I) = \begin{cases} e^{\left(\frac{V_I}{2} \times (I-7)\right)}, I \le 7 \\ 1, I > 7 \end{cases} \tag{6}$$

Table 4 summarizes the variable "Error", which means the difference between damage grades observed and damage grade estimated to 1669 buildings from Faial. "Damage grade estimated" was obtained through the mean damage grade (μ_D) calculating their mode (the value that occurs most frequently in a data set). The mode equation can be written as:

$$\text{mod}\, e = \left(\frac{8\mu_D - 5}{6}\right) \tag{7}$$

Table 4 - Comparison between damage observed and damage estimated - Faial

Intensity	Variable	N	Mean	StDev	SE Mean	95% CI
I (Matias *et al.*, 2007)	Error: obsv - estimated	1669	0.9353	1.4290	0.0350	(0.8667; 1.0039)
I (EPI 2)	Error: obsv - estimated	1669	0.9438	1.4543	0.0356	(0.8740; 1.0137)

Building damage estimates are crucial to derive damage scenarios using as starting points the seismic vulnerability and ground-shaking scenarios. Another method applied to analyse the observed damage was the expected damage defined by the average damage index (Dolce *et al.*, 1999):

$$DI_{med} = \sum_{1}^{5} \frac{d_i f_i}{n} \tag{8}$$

where d_i is a normalized damage grade (d_i = 1,…5, not null damage levels) and f_i the relevant frequency. DI_{med} ranges between 0 and 1, where DI_{med} = 0 is for total absence of damage and DI_{med} = 1 is for total destruction.

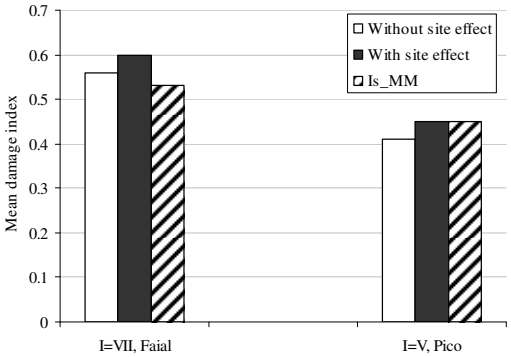

Figure 11: Mean damage index for the Faial and Pico islands: with and without site effect (Matias *et al.*, 2007), and derived from stochastic finite-fault simulation (EPI1)

On the whole territory of Faial and Pico island a mean damage index, DI_{med} (0–1 scale), has been obtained for the 1998 event, with and without taking into account site effects (Figure 11). This index does not represent the details of damage distribution, but is a synthetic tool to discuss the expected damage and allow a quick comparison among different scenarios.

Supposing a maximum intensity I_{MM}=VIII in Faial (see Figure 11) due to a soil amplification, we lower this value to I_{MM}=VII and describe it as site-effect dependent. The comparison between the mean damage index caused by the earthquake with and without soil amplification effects is shown Figure 11 where values for Faial are in the range of DI_{med}=0.53 -0.60 and DI_{med}= 0.41-0.45, respectively.

As can be observed in Figure 12, for each census tract ("freguesia") a DI_{med} was derived for Faial and Pico. The analyses in Faial shows a presence of three census tracts (Salão, Ribeirinha and Pedro Miguel) with DI_{med}= 0.60-0.80, where the most vulnerable buildings were concentrated with partial and total collapse.

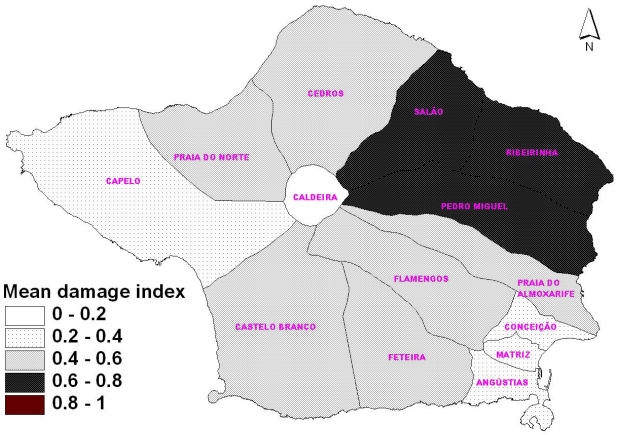

Figure 12: Mean damage index map for the Faial island for each census tract

A second evaluation of buildings damage was done using the simulation results with EPI2. An isoseismic map of this event is plotted in Figure 10 (right). Intensities and PGA values derived using EPI2 seem more reliable than those with EPI1. Moreover, using EPI2 is possible to reach maximum intensities of VIII in Faial.

Clearly, predicting site effects at a specific location is a complex task and was not included in this study. Here we only mean to contribute to the scatter between the predicted and observed values.

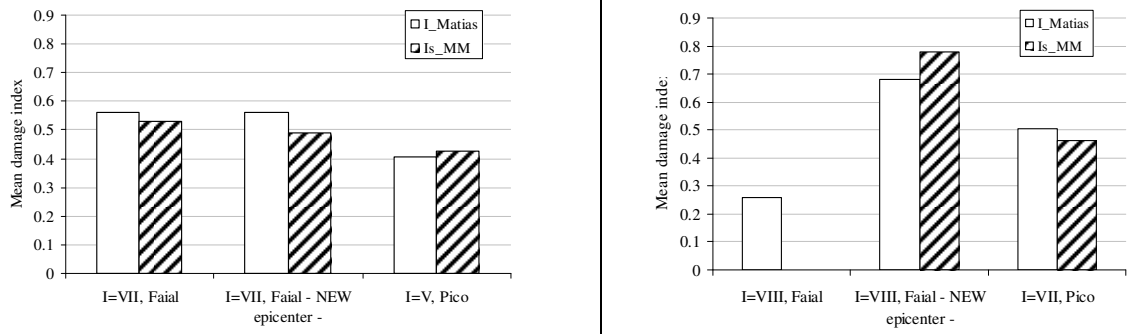

Figure 13: Mean damage index for two different scenarios: left panel shows intensity VII for Faial (EPI1 and EPI2= new epicenter) and V for Pico; right panel shows intensity VIII for Faial (EPI1 and EPI2= new epicenter)and VII for Pico. We compare mean damage index derived from (white) observed data (Matias *et al* , 2007) and (hatched) stochastic simulation.

7. PARAMETRIC ANALYSIS AT THE HORTA STATION

A parametric analysis of the finite-fault bedrock stochastic simulation at the Horta site was done to estimate the range of variation in amplitude and frequency. We grouped the parametric in two steps: the first step shows the influence of changes in rupture models, such as slip models (Figure 14) and nucleation points; the second step exploits the influence of quality factor Q(f) and stress drop, keeping fixed slip distribution and nucleation point.

Slip models are generated assuming a Gaussian distribution centred on nucleation points NP 1, NP 2 and NP 3, and NP 4 a random distribution generated automatically by EXSIM. The nucleation points are 4 for each slip model, and are located in the lower half of the fault. We have used in the simulation 16 rupture models (four nucleation points and four slip distributions) resulting in 480 stochastic time series, 120 time series for each slip model, at Horta site. We discuss the resulting ground shaking scenarios in terms of PGA only, but the same is valid for Response Spectrum Intensity (SI).

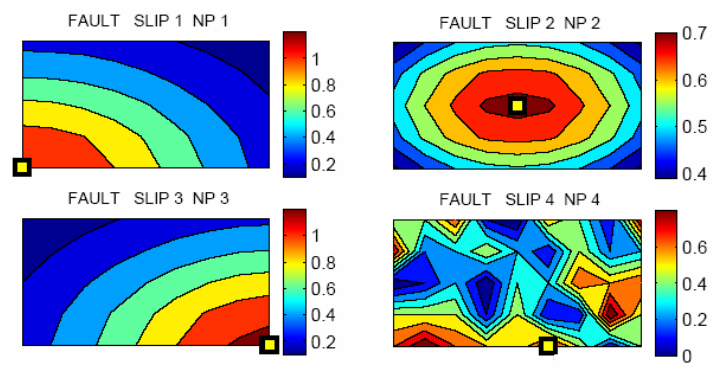

Figure 14: Slip distributions used in the parametric study at Horta site (Slip 1, Slip 2, Slip 3 and Slip 4). For each model 4 nucleation points are plotted (black-bold squares). Bottom right panel is the random slip distribution generated by EXSIM using the parameters listed in Table 4.

Crucial to the simulation is how close the maximum concentration of slip and nucleation point is to a given site. We calculate the median, the 75% and 84 % percentile, the mean, the mode, the minimum and maximum considering the maximum PGA for each time series. Values in Table 4, are maximum and mean PGA (cm/sec^2) derived from 30 simulated time series and different rupture models (combination of slip models with nucleation points).

Table 4 - Maximum and (mean) of the PGA (cm/sec^2) values simulated at the Horta site considering the 16 rupture models

Slip \ NP	NP 1	NP 2	NP 3	NP 4
SLIP 1	249.037 (198.858)	208.378 (170.609)	157.066 (141.964)	177.270 (159.411)
SLIP 2	295.362 (226.444)	269.723 (235.848)	223.165 (166.960)	271.974 (190.111)
SLIP 3	326.031 (273.537)	343.762 (259.360)	295.772 (244.029)	333.168 (269.847)-
SLIP 4	315.974 (262.984)	268.603 (252.424)	262.820 (218.858)	295.505 (240.424)

The highest PGA is for slip distribution SLIP 3. However higher PGA derived with NP 1, compared to those with NP 3, are caused by directivity. Another way to highlights what shown in Table 4 are the frequency PGA classes diagrams (Figure 15). The slip distribution SLIP 3 reveals a trend of frequency versus PGA class graphs (green values) shifted on higher class of PGA. In the background are PGA classes histograms (yellow bars) obtained considering all the rupture models. We can observe that the use of random distribution is a good choice when we have only little information on the slip distribution.

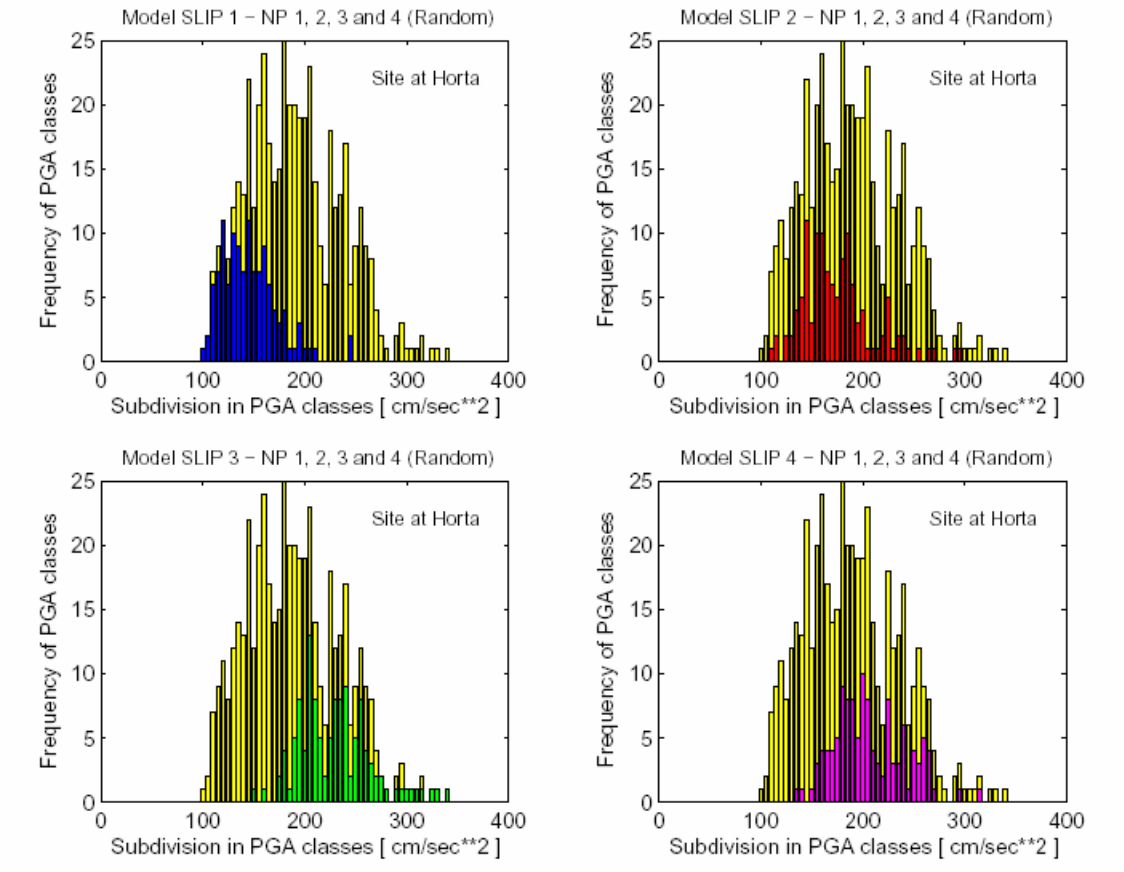

Figure 15: Frequency of PGA classes versus PGA computed from the 480 time series derived from all 4 slip models with scenario EPI 2 (yellow bars), and from the 120 time series derived from a single slip model (that are SLIP 1(blue), SLIP 2(red), SLIP 3(green) and SLIP 4(magenta).

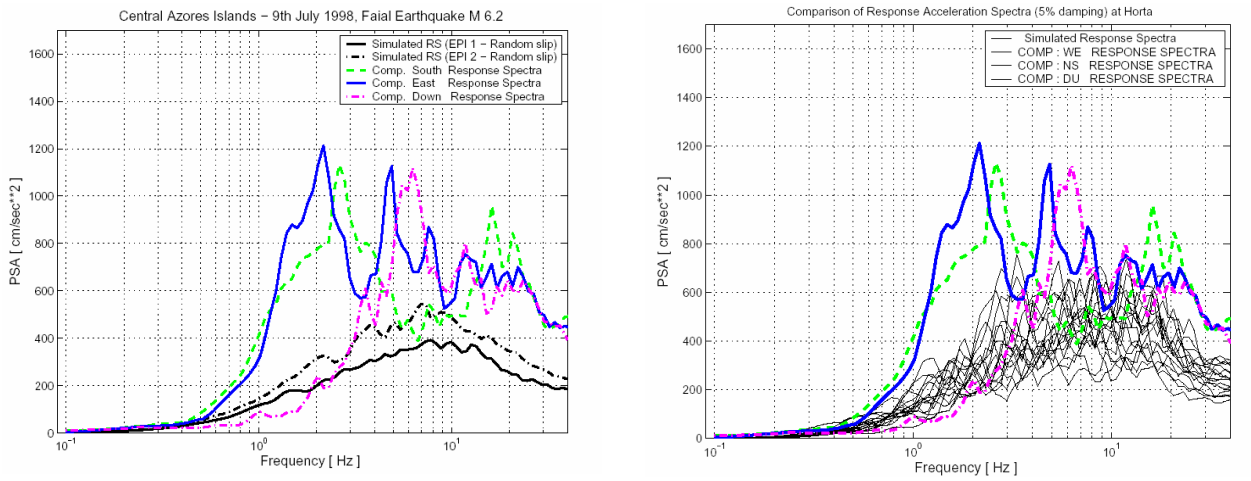

Figure 16: Recorded and simulated (in black) response acceleration spectra (5% damping) at Horta station. The digital recordings of the 9th July1998 Faial earthquake are in blue (WE), in green (NS) and magenta (DU).

In Figure 16, on the right are shown the response spectra from recorded (three components) with overlapped the simulated response spectra of the time series having the maximum value of PGA (on 30 trials) for each of 16 used models (Table 4 and Figure 16). The simulation has been done using the automatic random slip model assuming a bilateral rupture (NP 2), the parameters listed in Table 2 and the epicentre EPI 2 (Table 1). On the left of Figure 16 is shown the comparison between recorded and simulated response acceleration spectra. It shows that the suggested EPI 2 location fits better the response spectra from recorded data.

The next step will be to associate the time series with the PGA that matches the seven statistical values. In Figure 17 are plotted the 7 simulated series having as value of PGA matched with the value of the median, of 75% percentile, 84 % percentile, and of the mean, the mode, the minimum and the maximum. The time series have a very different behaviour in fact extended fault simulations produce high variability in the ground motion, which is mainly dependent on the slip distribution and on the assumed position of the hypocenter on the fault plane that controls the rupture directivity.

In Figure 17, on the bottom, are summarised the statistical values computed on the 480 values (Figure 15). The component EW of the accelerometer record of Horta is shown (red line) to compare it with the simulated time series.

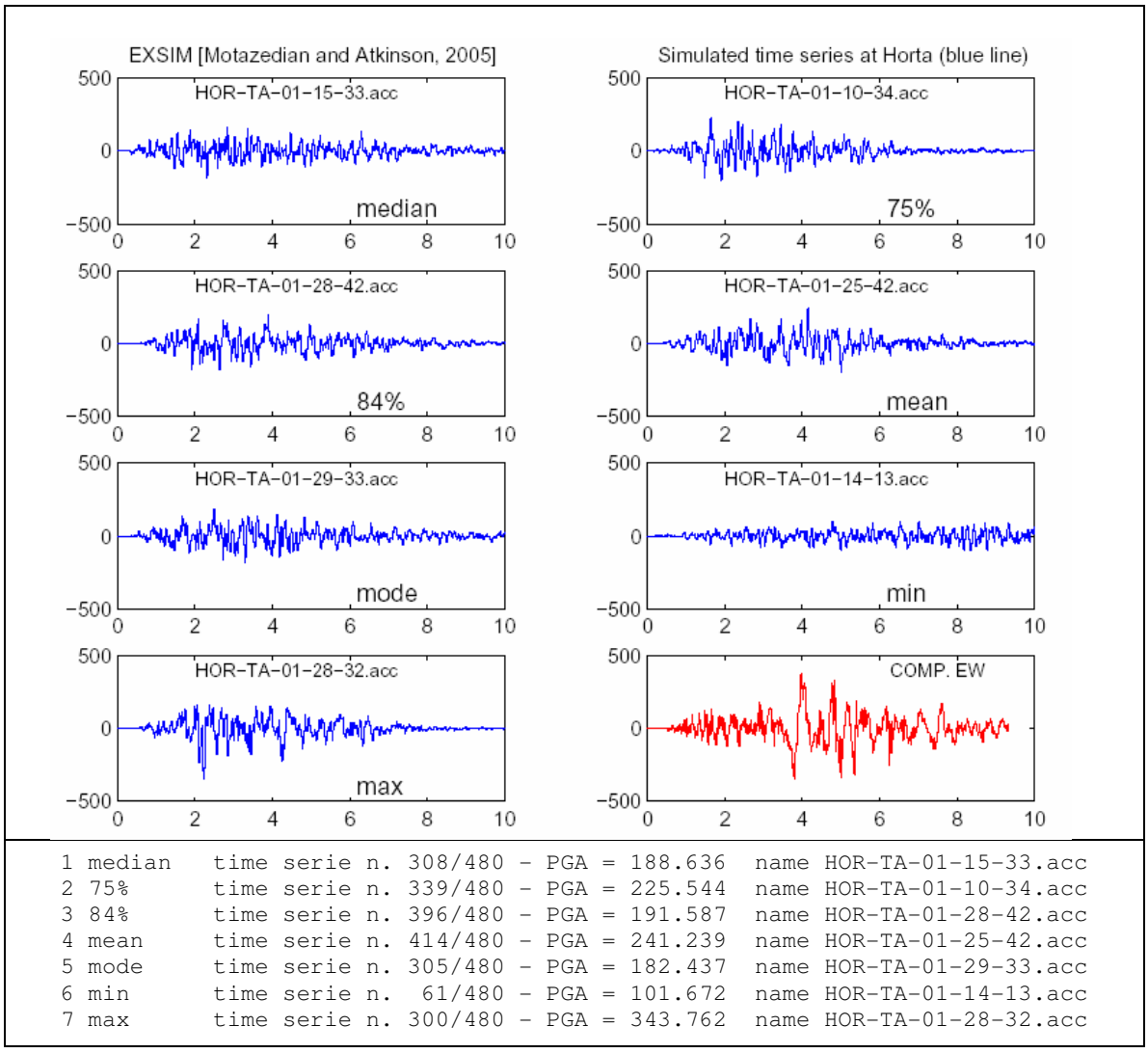


```
1 median   time serie n. 308/480 - PGA = 188.636  name HOR-TA-01-15-33.acc
2 75%      time serie n. 339/480 - PGA = 225.544  name HOR-TA-01-10-34.acc
3 84%      time serie n. 396/480 - PGA = 191.587  name HOR-TA-01-28-42.acc
4 mean     time serie n. 414/480 - PGA = 241.239  name HOR-TA-01-25-42.acc
5 mode     time serie n. 305/480 - PGA = 182.437  name HOR-TA-01-29-33.acc
6 min      time serie n.  61/480 - PGA = 101.672  name HOR-TA-01-14-13.acc
7 max      time serie n. 300/480 - PGA = 343.762  name HOR-TA-01-28-32.acc
```

Figure 17: Plots of the simulated time series derived with to the median, 75% and 84 % percentile, mean, mode, minimum and maximum PGA (cm/sec^2) . Lower right panel is the observed accelerogram (COMP. EW red line) at the Horta station.

We than discuss the simulation at the Horta site with Gaussian distribution and NP 2 (Figure 8), as a function of Qo and θ, in the attenuation relationship. We use EPI 2 and all the parameters listed in Table 2 to derive PGA and Intensity maps.

The shaking parameters shown in Figure 18 are:

- PGA
- the intensity $I_{MM\ (1)\ (PGA)}$ derived from relation (1) (Wald *et al.*,1999)
- the intensity $I_{MM\ (2)\ (PGV)}$ derived from relation (2) (Wald *et al.*,1999)

A combination between Qo (equal to 128, 239 and 425) and θ (equal to 1.06, almost linear frequency dependent, and equal to 0, no dependence with the frequency) arranged within 6 classes, have been used. Although class 1 and 3 results into calculated PGA closer to that measured at the Horta site, the same does not apply to what computed for the other islands.

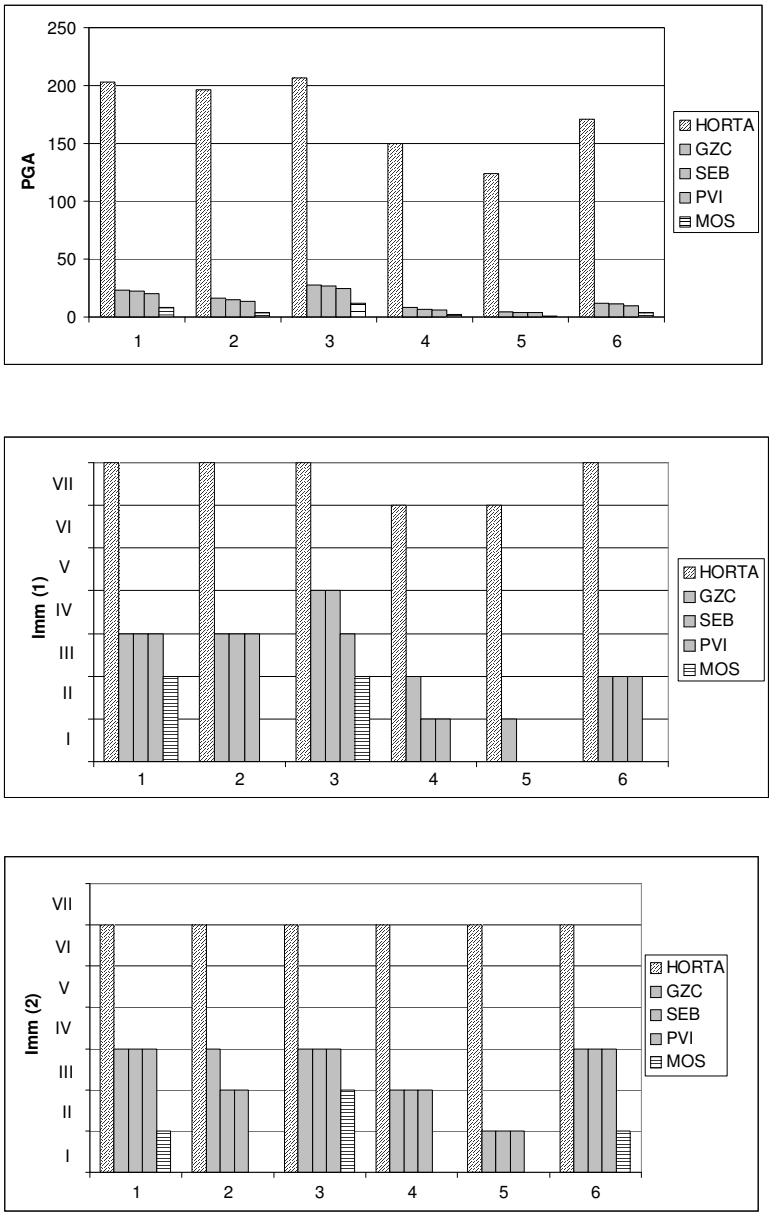

Figure 18: The stochastic simulations at Horta site combining different pair parameters Qo and θ parameters: 1) class 1 is for Qo = 239 and θ = 1.06; 2) class 2 is for Qo = 128 and θ = 1.06; 3) class 3 is for Qo = 425 and θ = 1.06; 4) class 4 is for Qo = 239 and θ = 0.0; 5) class 5 is for Qo = 128 and θ = 0.0; 6) class 6 is for Qo = 425 and θ = 0.0.
Top to bottom, plots PGA parameter, $I_{MM\,(1)}$ (derived from relation (1), Wald *et al.*,1999) and $I_{MM\,(2)}$ (derived from relation (2), Wald *et al.*,1999)

Therefore we suggest that class 1 (Qo=239 and θ=1.06) is a good compromise between the need to match the high PGA recorded at Horta site, and the low PGA at the Terceira and S. Miguel islands (see Table 1). $I_{MM(2)}$ does not seem to be a good way to derive intensity from shaking parameters, as it results from a two steps approximation: the derivation of PGV from PSA and, in turn the derivation of $I_{MM(2)}$ from PGV.

8. CONCLUSIONS

In the Central Azores Islands (Faial, Pico and S. Jorge) we have computed PGA and Intensity maps on a 0.02°x 0.02 grid using EXSIM program. To retrieve the Intensity we have used a PGA-intensity relationship (Wald *et al*., 1999). Stochastic damage finite-fault simulation has been generated using two epicenter locations scenarios, EPI 1 (Matias *et al*., 2007) and EPI 2 (this study).

Comparison of stochastic retrieved and observed intensity have been done for the Faial and Pico islands evaluating buildings damage and using a parametric analysis at the Horta site has been done as a function of model parameters

The stochastic simulations at the bedrock can not explain the content in amplitude and frequency of recorded ground motion at the Horta site. Nevertheless we discuss the limits of our analysis that in terms of input model parameters The damage index (Dolce *et al*., 1999) has been derived comparing values from stochastic scenarios (EPI 1 and EPI 2) and damage survey scenarios (Matias *et al*., 2007) in the Faial and Pico Island. Clearly part of the damage can be ascribed to localized ground motion amplification and inefficient construction practices. It is reasonable that surveyed intensities at some localities might be have a standard deviation one unit than the regional value plotted in maps.

9. ACKNOWDLEDGEMENTS

This study has been prepared for the International Seminar on Seismic Risk and Rehabilitation of Stone Masonry Housing and was funded by Instituto Superior Técnico and partially by Istituto Nazionale di Geofisica e Vulcanologia. The authors gratefully acknowledge the financial support of Fundação para a Ciência e a Tecnologia (SFRH/BD/29980/2006).

10. REFERENCES

Anderson, J.G. and Hough, S. E. (1984) A model for the shape of the fourier amplitude spectrum of acceleration at high frequencies. Bull. Seism. Soc. Am 74(5), 1969–1993.

Berardi, R., Jiménez, M. J., Zonno, G., García-Fernández, M. (2000) Calibration of stochastic finite fault ground motion simulations for the 1997 Umbria-Marche, Central Italy, earthquake sequence. Soil Dynamics and Earthquake Engineering 20, 315-324.

Beresnev, I.A., Atkinson, G.M. (1998) FINSIM - a FORTRAN program for simulating stochastic acceleration time histories from finite fault. Seism. Res. Lett. 69, 27-52.

Bommer, J.J., Alarcon, J.E. (2006) The prediction and use of peak ground velocity. Journal of Earthquake Engineering 10(1), 1–31.

Boore, D.M. (2003) Simulation of ground motion using the stochastic method. Pure Appl. Geophys. 160, 635-676.

Borges, J.F., Bezzeghoud, M., Buforn, E., Pro, C., Fitas, A. (2007) The 1980, 1997 and 1998 Azores earthquakes and some seismo-tectonic implications. Tectonophysics 435, 37–54.

Carmichael, S. R. (1990) Practical Handbook of physical properties of rocks and minerals. CRC press, Inc, 741.

Carvalho, A., Zonno, G., Franceschina, G., Serra Bilè, J., Campos Costa, A. (2008) Earthquake shaking scenarios for the metropolitan area of Lisbon. Soil Dynamics and Earthquake Engineering 28, 347-364.

Castro, R.R., Pacor, F., Franceschina, G., Bindi, D., Zonno, G., Luzi, L. (2008) Stochastic Strong-Motion Simulation of the Mw 6 Umbria-Marche Earthquake of September 1997: Comparison of Different Approaches. Bull. Seism. Soc. Am. 98(2), 662–670.

Catita, C., Catalão, J., Miranda, J. M., Mendes-Victor, L. A. (2008) Kinemetics of Faial-Pico Islands (Azores Archipelago) Deduced from Geodetic Surveys. To be published in 10 Years after the 1998 earthquake in the Azores, SPRHI, S.A.

Dias, N.A., Matias, L., Lourenço, N., Madeira, J., Carrilho, F. and Gaspar, J.L. (2007) Crustal seismic velocity structure near Faial and Pico Islands (AZORES), from local earthquake tomography. Tectonophysics 445, 301–317.

Dolce, M., Goretti, A. and Masi, A. (1999) Analisi dei danni causati dal sisma del settembre 1998 nel Pollino. Ingegneria Sismica, Anno XVI - N. 3, 5-15.

Fernandes, R.M.S., Miranda, J.M., Catalão, J., Luis, J.F., Bastos, L. and Ambrosius, B. (2002) Coseismic displacements of the Mw=6.1, July 9, 1998, Faial earthquake (Azores, North Atlantic). Geophys. Res. Lett. 29(16), 21/1–21/4.

Ferreira, M.A. (2008) Classificação dos danos no edificado com base na EMS-98. Sismo 1998 - Açores. Uma década depois. Edição C.S. Oliveira et al., Governo dos Açores/SPRHI, S.A.

Gallipoli M.R., Masi, A., Mucciarelli, M., Vona, M., Samela, L., Parolai, S., Strollo, A. and Gunther, E. (2007) Report of Tasks 5 and 7. Progetto S3 – Scenari di scuotimento in aree di interesse prioritario e/o strategico. http://esse3.mi.ingv.it/deliverables/ Deliverables_S3_D18_D19_D24.pdf, 99 pp.

Giovinazzi, S. and Lagomarsino, S., (2003) Seismic Risk Analysis: a Method for the Vulnerability Assessment of Built-up areas. Proceedings European Safety & Reliability Conference, Maastricht.

Giovinazzi, S., and Lagomarsino, S., (2002) A Method for the Vulnerability Analysis of Built-up areas. Proceedings International Conference on Earthquake Losses and Risk Reduction.

Grunthal, G. (1998) European Macroseismic Scale 1998. Cahiers du centre Eur. De Géodyn. Et de Séismologie, Vol. 15, 1-99.

Kramer, S. L. (1996) Geotechnical Earthquake Engineering. Prentice Hall, New Jersey.

Lourenço, N., Miranda J.M., Luís J.F., Ribeiro A., Mendes-Victor, L.A., Madeira, J. and Needham, H.D. (1998) Morpho-tectonic analysis of the Azores Volcanic Plateau from a new bathymetric compilation of the area. Mar. Geophys. Res. 20(3), 141-156.

Madeira, J. (1998) Estudos de neotectónica nas ilhas do Faial, Pico e S. Jorge: Uma contribuição para o conhecimento geodinâmico da Junção Tripla dos Açores. Ph.D. Thesis, Universidade de Lisboa, Lisboa (3), 537–546.

Madeira, J., Silveira, A.B. (2003) Active tectonics and first paleoseismological results in Faial, Pico and S. Jorge islands (Azores, Portugal). Annals of Geophysics 46(5), 733-761.

Madeira, J. and Silveira, A.B., Serralheiro, A. (1998) Efeitos geológicos do sismo do Faial de 9 de Julho de 1998. Protecção Civil (revista do Serviço Nacional de Protecção Civil) 14: 12-20.

Matias, L., Dias, N.A., Morais, A., Vales, D., Carrilho, F., Gaspar, J.L., Senos, L. and Silveira, A.B. (2007) The 9th July 1998 Faial Island (Azores, North Atlantic) seismic sequence. J. of Seismology 11, 275-298.

Motazedian, D. and Atkinson, G.M. (2005) Stochastic Finite-Fault Modeling Based on a Dynamic Corner Frequency. Bull. Seismol. Soc. Am 95(3), 995–1010.

Neves, F.; Costa, A.; Oliveira, C.S. (2007). Vulnerabiidade Sísmica do Parque Habitacional das Ilhas do Faial e Pico (Parte 1 - Danos Exteriores). Proceedings Sísmica 2007 - 7º Congresso de Sismologia e Engenharia Sísmica, Porto.

Neves, F.; Costa, A.; Oliveira, C.S. (2008). Vulnerabilidade Sísmica do Parque Habitacional das Ilhas do Faial e Pico. Sismo 1998 - Açores. Uma década depois. Edição C.S. Oliveira et al., Governo dos Açores/SPRHI, S.A.

Ólafsson, S., Sigbjörnsson R. and Einarsson, P. (1998) Estimation of Source Parameters and Q from Acceleration Recorded in the Vatnafjtll Earthquake in South Iceland. Bull. Sesmic Soc. Am. 88(2) 556-563

Oliveira C.S., Sigbjörnsson R. and Ólafsson S. (2004) A comparative study on strong ground motion in two volcanic environments: Azores and Iceland. 3th World Conference on Earthquake Engineering, Vancouver, B.C., Canada August 1-6, 2004, Paper No. 2369

Oliveira, C.S., Lemoş, J.V. and Sincraian G.E. 2002. Modelling Large Displacements of Structures Damaged by Earthquake Motions. European Earthquake Engineering, vol. 3, pp 56-71.

Pro, C. (2002) Estudio del efecto de directividad en la forma de ondas. Ph.D. Thesis, Universidad Complutense, Madrid, 259 pp.

Reches, Z. and Dieterich, J. H. (1983) Faulting of rocks in three-dimensional strain fields. I: Failure of rocks in poliaxial, servo control experiments. Tectonophysics, 95, 111-132.

Schilling, J.G. (1991) Fluxes and excess temperature of mantle plumes Inferred from their interaction with migrating mid-ocean ridges. Nature, 352, 397–403.

Senos, M.L., Gaspar, J.L., Cruz, J., Ferreira, T., Nunes, J.C., Pacheco, J.M., Alves, P., Queiroz, G., Dessai, P., Coutinho, R., Vales, D. and Carrilho, F. (1998) O terramoto do Faial de 9 de Julho de 1998. 1° Simpósio de Meteorologia e Geofísica da APMG Lagos, 61–67.

Silveira, G., Stutzmann, E., Davaille, A., Montagner, J.P., Mendes-Victor, L. and Sebai, A. (2006) Azores hotspot signature in the upper mantle. J. Volcanology and Geothermal Research, 156, 23–34.

Udias, A., Lopezarroyo, A. and Mezcua, J. (1976) Seismotectonic of Azores–Alboran region. Tectonophysics 31(3–4), 259–289.

Vogt, P.R. (1976) Plumes, Subaxial Pipe-Flow, and Topography Along Mid-Oceanic Ridge. Earth and Planetary Science Letters, 29(2), 309–325.

Wald D.J., Quintoriano V., Heaton T.H. and Kanamori H. (1999) Relationships between Peak Groung Acceleration, Peak Ground Velocity, and Modified Mercalli Intensity in California in California. Earthquake Spectra, 15, (3), 557-564.

Watson, D.F. and Philip, G.M. (1985) A Refinement of Inverse Distance Weighted Interpolation. Geoprocessing, 2, 315-327.

Wells, D.L. and Coppersmith, K. J. (1994) New empirical relationships among magnitude, rupture length, rupture width, rupture area, and surface displacement. Bulletin of the Seismological Society of America 84, 974-1002.

Yang, T., Shen, Y., Van der Lee, S., Solomon, S. C. and Hung, S. H. (2006) Upper mantle structure beneath the Azores hotspot from finite-frequency seismic tomography. Earth and Planetary Science Letters 250, 11–26.